STUDY OF THE BEHAVIOUR OF SLAB-COUPLED T-SHAPED RC WALLS

E. Smyrou[1], T.J. Sullivan[2], M.J.N. Priestley[3] and G.M. Calvi[4]

[1] *PhD Candidate, Centre of Research and Graduate Studies in Earthquake Engineering and Engineering Seismology (Rose School), Pavia, Italy*
[2] *Assistant Professor, Dept. of Structural Mechanics, University of Pavia, Pavia, Italy*
[3] *Professor, Centre of Research and Graduate Studies in Earthquake Engineering and Engineering Seismology (Rose School), Pavia, Italy*
[4] *Professor, Centre of Research and Graduate Studies in Earthquake Engineering and Engineering Seismology (Rose School) & Dept. of Structural Mechanics, University of Pavia, Pavia, Italy*
Email: smiroulena@gmail.com

ABSTRACT :

In this paper, a number of 3-dimensional nonlinear finite element models of two T-shaped walls coupled by slab are created using 2-dimensional elements, varying in each one the slab width. Related modelling issues are discussed. Nonlinear static analysis is employed in an attempt to determine the effective slab width. By means of studying the rotations and the strain field originated, a simple preliminary expression for the effective slab width is proposed. Attention is focused on the deflected shape of the slab and the areas in which high strains are recorded. A sensitivity analysis is conducted in order to evaluate the relative importance of factors such as the width, the reinforcement percentage and the thickness of the slab on the width of effective slab. The results indicate that the slab thickness and reinforcement may have a negligible influence on the effective slab width. The uncertainties associated with the effective width concept are discussed and the needs of future research identified.

KEYWORDS: T-shaped walls, slab coupling, nonlinear static analysis, effective slab width

1. MOTIVATION

A common form of construction for high-rise buildings consists of RC walls connected solely through floor slabs, producing an efficient structural system. Despite its wide applicability, the interaction of RC walls connected by slabs has not attracted significant research interest, resulting in relatively limited publications. Relevant publications are typically based on linear elastic theory and uncracked slab sections (Coull and Choudhury, 1967; Qadeer and Stafford Smith, 1969), while a couple of experimental studies can be located (Schwaighofer and Collins, 1977; Paulay and Taylor, 1981). Moreover, the case of slab-coupled T-shaped walls with opposite facing interior flanges forming a corridor area between them, though frequently met in hotels and apartments buildings, has been rarely examined (Coull and El Hag, 1975; Tso and Mahmoud, 1977, Coull and Wong, 1984).

The principles for conventionally beam-coupled walls could be applied in the case of slab-coupled walls under the assumption that the slab works as a wide coupling beam. Due to its complex behaviour, the slab is simulated with a simple one-way strip possessing a certain equivalent width, an approximation that allows satisfactory precision when considering the difficulties introduced by complex nonlinear behaviour. The concept of the effective slab width, borrowed from the design of T-beams (Pantazopoulou et al., 1988) and adapted to the needs of this study, aims to replace the actual slab with a slab-beam element that rotates uniformly across its transverse width. Its thickness will be that of the slab and its width equal to a fraction of the actual slab transverse width. Full coupling between the walls is expected along the flanges, so the question that needs to be answered is what width of slab participates beyond the flange ends and between adjacent walls. To study this, a number of analytical models of slab-coupled T-shaped RC walls are constructed in order to investigate the effect of a number of other parameters on the width of effective slab that are involved in the coupling of the walls. For this purpose, advanced software tools and nonlinear analysis are employed, with special focus on modelling aspects.

2. NUMERICAL MODELS

2.1. Description of Case Study Models

Considering the case of a hotel, where subsequent walls define the space of each room and the distance between their flanges is partly used for accommodating the door opening, the amount of the slab participating on both sides of each wall could be expected to be dependant on the distance between subsequent walls. If this distance is relatively short, coupling in the two directions of the principal axes of the flange is expected and then the whole slab will contribute. The part of the structure that was modelled in the general-purpose finite element program ABAQUS (2007) contains the two T-shaped walls with opposite-facing flanges, coupled by their flanges, and the surrounding slab until the mid-distance between subsequent walls (indicated in Figure 1a). Free boundary conditions were assigned for the slab, the total width of which varied between 4 and 20m.

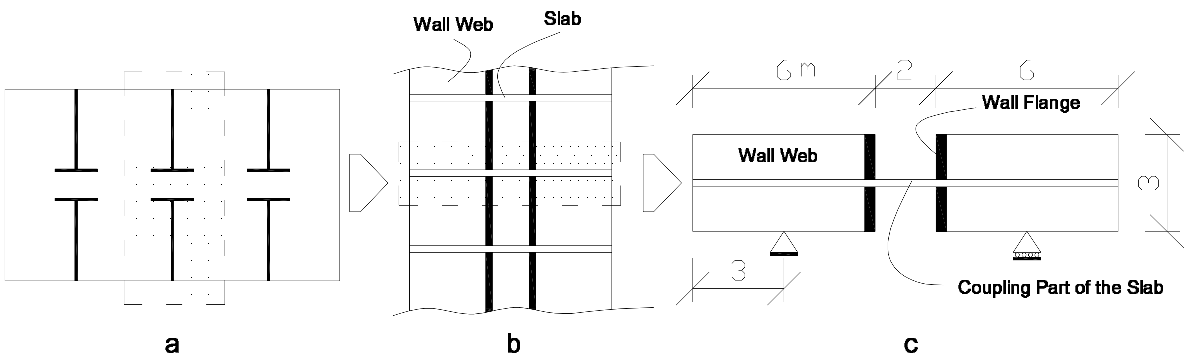

Figure 1 (a) Plan of the case study structure considered, (b) Cross-section of the slab-coupled T-shaped walls and (c) the simplified model

The dimensions of the T-shaped walls were kept constant in all models, as the flange width was not included as a variable in this study. A T-shaped wall of web-flange ratio equal to 2.0 was selected with 6m web length and 3m flange width, dimensions commonly met in real structures. The width of the corridor between opposite walls was equal to 2m in all models, since in reality it is not expected to vary considerably due to architectural reasons. Another parameter the effect of which was examined is the slab thickness, for which the values of 150mm and 200mm were assigned.

The reinforcement of the slab was uniform, without special provisions for specific areas and equal to 0.2, 0.5 and 1.0%. Upper reinforcement was used near the supports (as such the wall webs and flanges are regarded) and distribution reinforcement was placed too. In the analysis it was assumed that no buckling of the reinforcement will occur, though in reality the rebars in certain regions, such as those adjacent to the walls flanges, may need to be protected against buckling as they tend to undergo significant strains.

The T-shaped walls were modelled 3m high, representing the distance between mid-height points of successive storeys, where zero moments are expected (Figure 1c). One wall was pinned, while the other was supported on a pinned roller, allowing thus the elongation of the coupling part of the slab. This may be representative of upper levels of buildings where significant coupling might be expected. Future work could establish the differences one might expect when the walls are restrained laterally with respect to each other. Nonlinear static analysis was conducted by applying displacement at the top of the walls. Thus, the walls rotate equally without deforming, unlike the slab connecting the wall flanges which is subjected to double bending due to the walls' rotation. More distant parts of the slab do not experience the same rotation, though they may be under bi-directional action. Such configuration decouples the behaviour of the walls from that of the slab. The walls remain elastic, while the slab in certain regions is under high ductility demand. Walls have been pushed until 3% drift. The slab drift is calculated as a function of the wall drift since the walls are forced to rotate over a certain point. The geometric relationship is given by

$$\theta_C=\theta_w\,(1+l_w/L_c) \tag{2.1}$$

where l_w and L_c are the wall length and the corridor width, θ_C is the rotation of the coupling part of the slab and θ_W is the rotation of the wall. For the case study walls, Eqn. 2.1 yields to a drift value for the coupling slab equal to four times the wall drift.

2.1. Modelling Issues

In total, 52 finite element models were analysed. For detailed description of the models, the reader is referred to Smyrou (2008). The models were created by using 4-node shell elements meshed with 0.20m edge length (Figure 2). Well-confined concrete material is assigned only for wall sections, while slightly-confined concrete material is used for the definition of the slab elements. Concrete of 30MPa compressive strength is used, the steel yield stress is assumed as 450MPa and steel hardening is taken into account. Rigid strips, approximately 300 times more rigid than the wall sections, are defined at the top and bottom of the wall members in order to homogenize the concentrated stresses caused by the point supports.

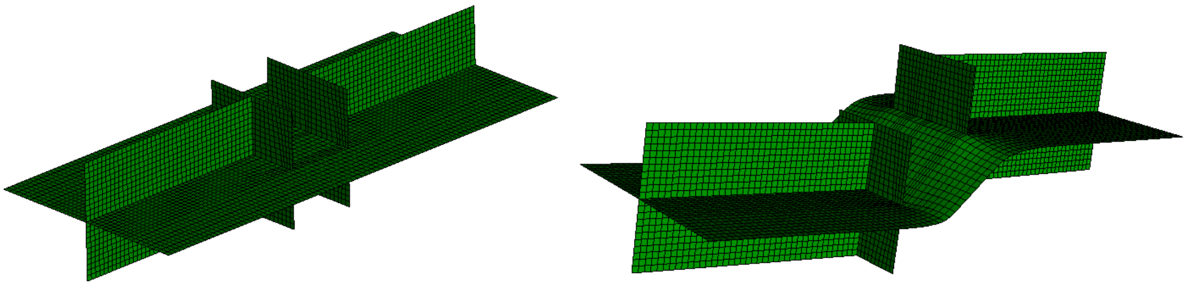

Figure 2 Meshed un-deformed (left) and deformed shapes (right) of one case study model

The non-linear behaviour of concrete is modelled using the concepts of classical plasticity, provided that an adequate yield function is introduced in order to reflect the different response of concrete under tension and compression (Mahrenholtz et al., 1982; Arslan, 2007). For this purpose, tension and compression hardening are defined separately and composite sections are introduced to the meshed elements. Specifically, the composite sections comprise elasto-plastic steel bars and two material models for concrete using Drucker-Prager yield surface (Drucker and Prager, 1952), accounting for compression hardening and tension hardening respectively.

Several models exist representing the real position of the reinforcement within the concrete layers (Hand et al., 1973, Phuvoravan and Sotelino, 2005). Some models propose a combination of 4-node Kirchhoff elements with 2-node Euler beams connected with rigid links, while others suggest a layered composite approach according to which the smeared rebars are inserted between two concrete layers. Defining the rebar can be tedious in complex problems, but it is important that it is done accurately, since it may lead to failure of the analysis due to lack of reinforcement in key regions of the model. Reinforcement bars are simulated with 1-dimensional strain theory elements (rods) that can be defined singly or embedded in oriented surfaces. In this study, rebars are defined by elasto-plastic material and are superposed on a mesh of standard shell elements used to model the concrete. The reinforcement is assumed smeared. Effects associated with the rebar/concrete interface, such as bond slip and dowel action, or bar buckling effects are neglected and their influence could be considered in future work.

3. ANALYSES RESULTS

3.1. Pushover Curves

The overall behaviour of the part of slab between the wall flanges is presented by means of force-displacement curves. Because of space limitations, only the pushover plots obtained for the models with 0.20m slab thickness and reinforcement equal to 0.2% and 0.5% are given in Figure 3. The other results can be found in Smyrou (2008). The vertical axis represents the vertical reaction force at the support restraining one of the walls. Note that the support reactions are the resultant of the imposed drift and are equal with opposite signs for the two walls. As readily noticed, all the curves characteristically exhibit yield at 1% drift, independently of the reinforcement level and slab width L_S. Another important observation is the tendency for the post-yield stiffness ratio to start with negative values where the slab width is relatively small (i.e. 4, 5 or 6m) and gradually pass to positive ratios. This change can be explained by considering that the slab parts remaining in the pre-yield phase increase and still contribute to the overall response of the slab.

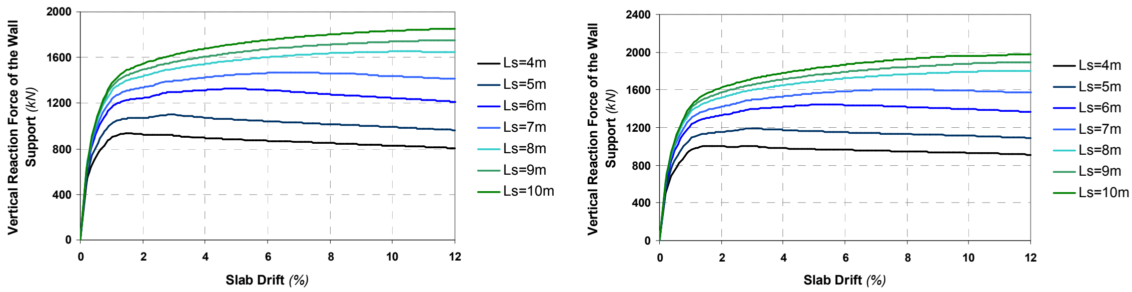

Figure 3 Example pushover plots for the case of 0.2m slab thickness and 0.2% (left) and 0.5% (right) slab reinforcement ratios

3.2. Limit-States

The values of rotations are extracted for each analysis for two limit-states, i.e. yield and ultimate, which were defined according to suggestions by Priestley et al. (2007). The expressions are addressed for conventionally reinforced coupling beams but are used in order to estimate the yield and the ultimate drift, under the condition that the behaviour of the coupling part of the slab can be simulated as a wide beam despite its low depth. So, the yield drift of a conventionally reinforced coupling "beam" was computed by

$$\theta_{C,y} = 0.5\ \phi_{yC}\ (0.5L_C + L_{SP})(1+F_v) \tag{3.1}$$

where L_{sp} is the strain penetration depending on the steel yield stress and the diameter of the re-bars. F_v is a flexibility coefficient to approximately allow for additional shear deformation and its value is related to the coupling "beam" aspect ratio. Specifically, $F_v=3(h_C/L_C)^2$, where h_C and L_C are the section depth and the length of the "beam", respectively. Finally, ϕ_{yC} is the yield curvature obtained by using the simplified expression by Priestley et al. (2007) for rectangular beams.

Moreover, assuming that buckling is prevented by proper reinforcement, which will also delay crushing of concrete, the tensile strain limit of the rebars governs the plastic rotation capacity. Taking the distance from the centroid of tensile reinforcement to neutral axis equal to 80% the slab thickness h_c, the rotation capacity for the damage-control limit of the coupling part of the slab is approximated by

$$\theta_{C,u} = 0.6\varepsilon_{su} \cdot 2L_{sp} / (0.8h_C) \qquad (3.2)$$

where ε_{su} is the ultimate strain of steel taken as 10%. Note that the coupling part of the slab will be critical, i.e. will yield and reach the ultimate rotation, because in the model the walls remain elastic. Finally, it is underlined that the aforementioned calculations, though necessary in order to correlate the progressive deformation of the slab (Figure 4) to certain limit-states, should be treated with caution as indicative approximations. As shown by the analysis results hereinafter, the error caused by this assumption did not affect the calculations for the effective slab width.

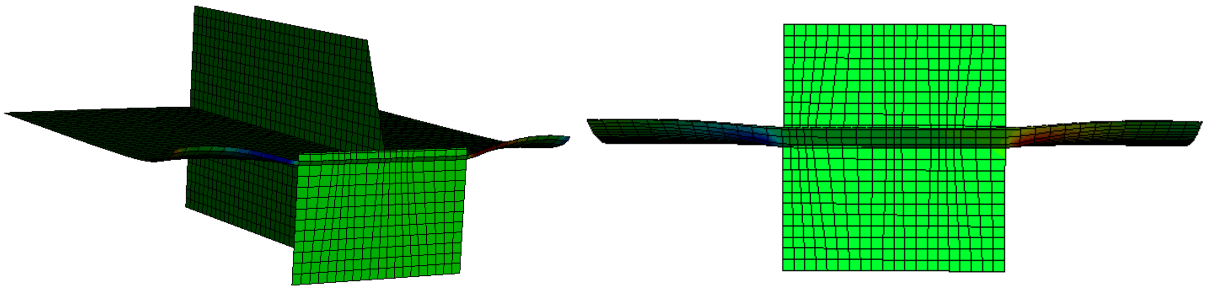

Figure 4 Perspective view and cross-section parallel to flanges showing the deformed slab

3.3. Estimation of Effective Slab Width

There is no constant criterion for the definition of the effective width of the slab L_{eff} (Hwang and Moehle, 2000; Pantazopoulou and French, 2001), which may be based on forces or deformations. In this study, the effective width of the slab is determined by assuming uniform rotations along L_{eff}, after which the contribution of the slab can be regarded as negligible. Therefore, two paths, one for each flange, were defined in each model, having length equal to L_s and being parallel and next to the flanges (Figure 5). The rotations of the shell elements along the paths are recorded for each step of the analysis. The rotations about the axis perpendicular to the flanges are tracked, the absolute values of which peak on both sides of the flange right after the flange tips and reduce over a short length (Figure 5). The same curve of rotations along the slab width is obtained for all steps of analysis but, as expected, with different magnitude.

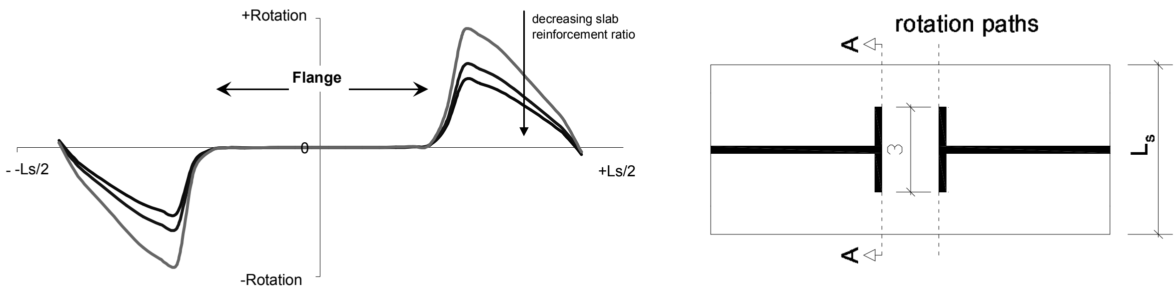

Figure 5 Schematic view of the rotations about the specifies path perpendicular to flanges

The approach followed in this study for the effective slab width is to equilibrate the work required by the slab to develop and afterwards to recover the imposed rotations. The rotation values are significant until a point, which needs to be determined, and fade out gradually after that certain point. The equilibrium process is shown in Figure 6. The rectangular width equal to the distance of the end of the slab from the point the maximum rotation occurs is set a height such that its area balances the area of the two triangles A. As soon as the intersection point of the rotation curve with the rectangle is located, then the effective slab width is estimated. Specifically, the effective width of the slab is thus the sum of L_A doubled and the flange width, which is 3m in the models examined.

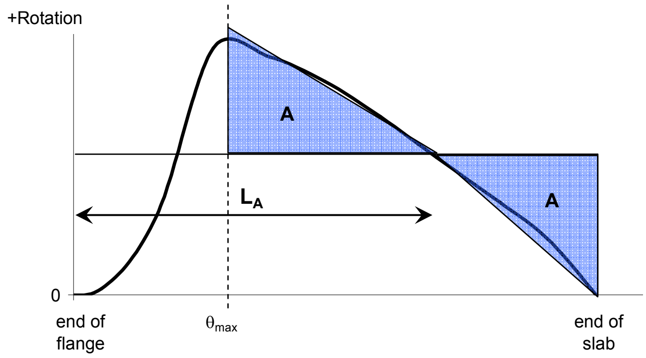

Figure 6 Definition of L_A based on energy equilibrium

The application of the above described method leads to the results given in Figure 7. The effective slab width (flange width plus two times L_A) is defined as a function of the actual slab width, L_s. The effective slab width increases linearly with the slab's total width, as shown by Eqn. 3.3.

$$L_{eff} = 2.10 + 0.41L_S \tag{3.3}$$

Note that the units in Eqn.3.3, the graphical representation of which is given in Figure 7, are in meters. It is underlined that the expression of L_{eff} was derived for a specific flange width. It is emphasised that Eq. 3.3 is a preliminary expression for the effective slab width and alternative means of evaluating the effective slab width could lead to a different relationship. It is clear that the slab does deform in a 3-dimensional manner and, because of the limited scope of this investigation, this study has only considered slab rotations about an axis parallel to the flanges. Future work will consider rotations about the perpendicular axis and will investigate the effective width values obtained when the axial forces developed in the walls are used to back calculate the effective slab width. Furthermore, the influence of the flange width on the distance will be studied.

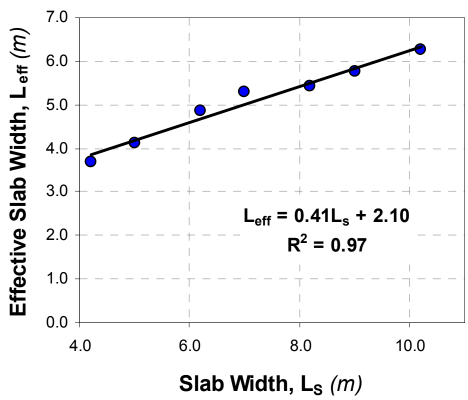

Figure 7 Effective slab width as a function of slab width, L_S

For the slab effective width definition adopted, the results clearly indicate that the L_{eff} remains unaffected by the reinforcement content and the thickness of the slab, exhibiting striking stability when these two parameters varied. Finally, the estimation of the effective slab width was not affected by the rotation step output selected. The slab rotates around a specific point, the location of which is not influenced by the magnitude of the rotations recorded and instead remains constant for all the steps of the analysis, giving the same value for the effective slab width at yield and ultimate limit-state steps.

3.4. Strain Field

The development of strains has also been investigated to highlight the behaviour of the most deformed regions of the slab. A snapshot from the ultimate step of an analysis is given in Figure 8, where only the regions close to the flanges are coloured. In the case presented, the slab width, L_S, is 6m, the slab section depth is 0.15m and the slab reinforcement ratio is equal to 0.2%. Strain values are plotted for the outermost leaf of the core section at the bottom face of the slab.

The maximum tensile strains, which are up to 8.3%, are observed in the slab parts adjacent to the left flange in a very narrow (around 10cm) strip along the flange. This is the region the highest rotation demand is expected. Strain values diminish to 3% within the effective width suggested in this research work. The compression zone which causes crushing of the concrete propagates even behind the flange and covers a considerable area. Maximum compressive strain increases up to 2.8% in a very narrow strip parallel to the right flange. However, compressive strains diminish quickly to 1%. The compressive strains recorded indicate that if slab integrity is to be maintained special confinement would be needed around the flanges tips and in an area behind the flanges, the length of the effective width. This special reinforcement may consist of cages that will create a confined zone in this region.

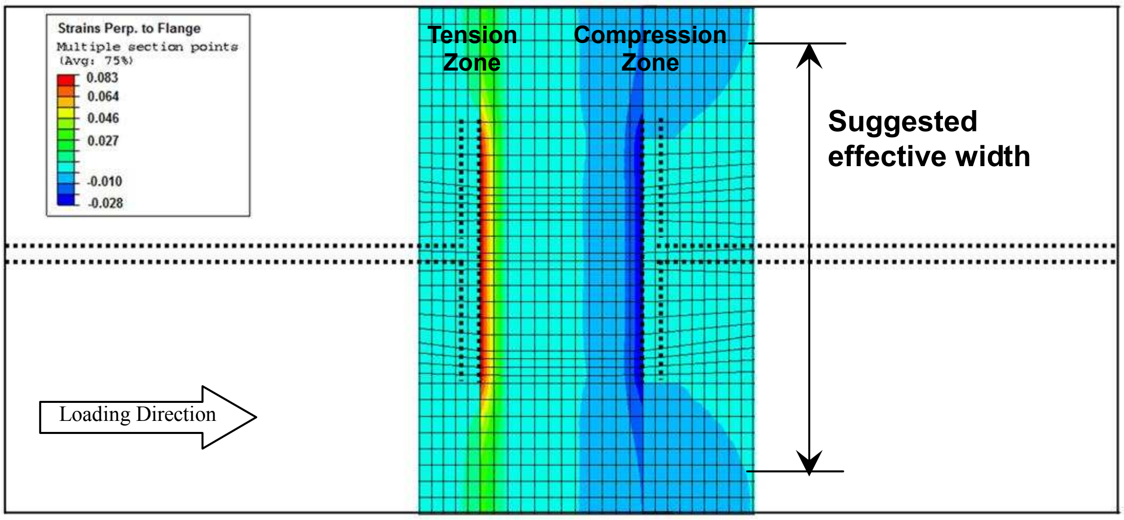

Figure 8 Strains perpendicular to flanges at the bottom face of the slab

4. CONCLUSIONS

After a brief literature review the need for studying the behaviour of slab-coupled T-shaped walls by means of advanced software tools, employing nonlinear analysis, arose. 3-dimensional finite element models of slab-coupled T-shaped walls were constructed, representing a commonly met structural system. The models, consisting of two T-shaped walls with opposite-facing flanges, coupled by the surrounding slab until the mid-distance between subsequent walls, were subjected to nonlinear static analysis. Details on the modelling aspects and assumptions were presented. The main aim of this work was to estimate the amount of slab participating in coupling action. The approach of effective slab width was utilised. A definition of the effective slab width within the needs of this work, as well as an attempt to define reasonable limit-states despite the inherent difficulties, was described. The rotations along predefined paths on the slab were monitored, exhibiting in all models the same shape that was characterised by peak rotation values close to flange ends decreasing over a short length. A simple preliminary expression for the calculation of the effective slab width as a function of the total slab width was provided, underlining, nevertheless, the need for further research on case study T-shaped walls with variable flange width. Pushover plots, relating the support reaction to the drift level at each step of the analyses, were produced. The influence of parameters such as the slab thickness and slab reinforcement on the effective slab width, was found to be negligible. The strain field produced showed that the most affected regions of the slab extend along the wall flange faces until the end of the effective slab width. Moreover, the areas around the flanges tips in the compressive side of the coupling part of the slab experienced high strains, highlighting the necessity for special reinforcement.

REFERENCES

ABAQUS (2007). ABAQUS – Version 6.6.1, Inc., Pawtucket, R.I.

Arslan, G. (2007). Sensitivity study of the Drucker-Prager modelling parameter in the prediction of the nonlinear response of reinforced concrete structures. *Materials and Design* **28**, 2596-2603.

Coull, A. and Choudhury, J.R. (1967). Stresses and deflections in coupled shear walls. *ACI Journal Proceedings* **64:2**, 65-72.

Coull, A. and El Hag, A.A. (1975). Effective coupling of shearwalls by floor slabs. *ACI Journal Proceedings* **72:8**, 429-431.

Coull, A. and Wong, Y.C. (1984). Stresses in slabs coupling flanged shear walls. *ASCE Journal of Structural Engineering* **110:1**, 105-119.

Drucker, D. C. and Prager, W. (1952). Solid mechanics and plastic analysis for limit design. *Quarterly of Applied Mathematics*, **10:2**, 157-165.

Hand, F.R., Pecknold, D.A. and Schnobrich, W.C. (1973). Nonlinear layered analysis of RC plates and shells. *Journal of the Structural Division ASCE* **99:7**, 1491-1505.

Hwang, S.J. and Moehle, J.P. (2000). Models for laterally loaded slab-column frames. *ACI Structural Journal* **97:2**, 345-352.

Mahrenholtz, O., Reddy, D.V. and Bobby, W. (1982). Limit analysis of internally pressurized cut-and-cover type underground reactor containments. *ACI Journal* **79,** 219-231.

Pantazopoulou, S.J. and French, C.W. (2001). Slab participation in practical earthquake design of reinforced concrete frames. *ACI Structural Journal* **98:7**, 479-489.

Pantazopoulou, S.J., Moehle, J.P. and Shahrooz, B.M. (1988). Simple analytical model for T-beams in flexure. *Journal of Structural Engineering ASCE* **114:7**, 1507-1523.

Paulay, T. and Taylor, R.G. (1981). Slab coupling of earthquake-resisting shearwalls. *ACI Journal Proceedings* **78:2**, 130-140.

Phuvoravan, K. and Sotelino, E.D. (2005). Nonlinear finite element for reinforced concrete slabs. *Journal of Structural Engineering* **131:4**, 643-649.

Priestley, M.J.N., Calvi, G.M. and Kowalsky, M.J. (2007). Displacement-based seismic design of structures, IUSS press, Pavia, Italy.

Qadeer, A. and Stafford Smith, B. (1969). The bending stiffness of slabs connecting shear walls. *ACI Journal Proceedings* **66:6**, 464-473.

Smyrou, E. (2008). Seismic design of T-shaped RC walls, PhD Thesis, Rose School, IUSS press, Pavia, Italy (in preparation).

Schwaighofer, J. and Collins, M.P. (1977). Experimental study of the behaviour of reinforced concrete coupling slabs. *ACI Journal Proceedings* **74:3**, 123-127.

Tso, W.K. and Mahmoud, A.A. (1977). Effective width of coupling slabs in shear walls buildings. *Journal of the Structural Division, ASCE*, **103:ST3**, 573-586.